Otology & Neurotology
38:441–447 © 2017, Otology & Neurotology, Inc.

Cadaveric Testing of Robot-Assisted Access to the Internal Auditory Canal for Vestibular Schwannoma Removal

*Neal P. Dillon, †Ramya Balachandran, ‡Michael A. Siebold, *Robert J. Webster III, †George B. Wanna, and †Robert F. Labadie

Mechanical Engineering; †Otolaryngology, Vanderbilt University Medical Center; and ‡Electrical Engineering, Vanderbilt University, Nashville, Tennessee

Hypothesis: An image-guided robotic system can safely perform the bulk removal of bone during the translabyrinthine approach to vestibular schwannoma (VS).

Background: The translabyrinthine approach to VS removal involves extensive manual milling in the temporal bone to gain access to the internal auditory canal (IAC) for tumor resection. This bone removal is time consuming and challenging due to the presence of vital anatomy (e.g., facial nerve) embedded within the temporal bone. A robotic system can use preoperative imaging and segmentations to guide a surgical drill to remove a prescribed volume of bone, thereby preserving the surgeon for the more delicate work of opening the IAC and resecting the tumor.

Methods: Fresh human cadaver heads were used in the experiments. For each trial, the desired bone resection volume was planned on a preoperative computed tomography (CT) image, the steps in the proposed clinical workflow were undertaken, and the robot was programmed to mill the specified volume. A postoperative CT scan was acquired for evaluation of the accuracy of the milled cavity and examination of vital anatomy.

Results: In all experimental trials, the facial nerve and chorda tympani were preserved. The root mean squared surface accuracy of the milled cavities ranged from 0.23 to 0.65 mm and the milling time ranged from 32.7 to 57.0 minute.

Conclusion: This work shows feasibility of using a robot-assisted approach for VS removal surgery. Further testing and system improvements are necessary to enable clinical translation of this technology. **Key Words:** Bone milling—Image-guidance—Mastoidectomy—Robotic surgery—Translabyrinthine approach—Vestibular schwannoma.

Otol Neurotol **38:**441–447, 2017.

Vestibular schwannomas (VS) are benign tumors of the vestibular nerve located in the internal auditory canal (IAC) and extending into the cerebellopontine angle (CPA) that can cause partial or complete unilateral hearing loss, dizziness and loss of balance, facial weakness, tinnitus, and headaches, among other symptoms. Due to the benign and slow growing nature of VS, there is a trend in the United States and worldwide toward less invasive treatment (1) (e.g., observation and radiotherapy); however, many patients require some form of surgical intervention, especially in cases where the tumor is large, radiotherapy is not effective, or the tumor is causing substantial discomfort for the patient. The translabyrinthine approach is a common procedure for VS removal and is generally preferred (compared with other approaches such as the retrosigmoid and middle fossa) in cases when the the tumor is large, it extends into the CPA, or the patient has little remaining hearing (2).

Extensive bone removal is required to reach the IAC using the translabyrinthine approach (Fig. 1). The mastoid and the labyrinth are milled away and the bone covering the IAC and posterior fossa is thinned to the thickness of an egg shell allowing this small amount of remaining bone to be carefully removed manually to access the IAC (2). Following the opening of the IAC, the tumor is carefully separated from the nerves and removed. Obliterating the mastoid and labyrinth using a hand-held drill can take several hours because vital anatomy (e.g., the facial nerve) is embedded within the bone and must be identified and avoided. Given the challenging and time consuming nature of this task, we hypothesize that using a robot for the bulk bone removal portion of the surgery would be time and energy efficient as it would preserve the surgeon's energy and

Address correspondence and reprint requests to Neal P. Dillon, M.S., Vanderbilt University, PMB 351592, 2301 Vanderbilt Place, Nashville, TN 37235; E-mail: neal.p.dillon@vanderbilt.edu

Financial support: This work was supported by Award Number R01 DC012593 from the National Institute on Deafness and Other Communication Disorders (NIDCD) of the National Institutes of Health (NIH) and an unrestricted educational grant from Medtronic who donated the Midas Rex drill used in the experimentation. The content is solely the responsibility of the authors and does not necessarily represent the official views of the NIDCD or NIH.

The authors disclose no conflicts of interest.

DOI: 10.1097/MAO.0000000000001324

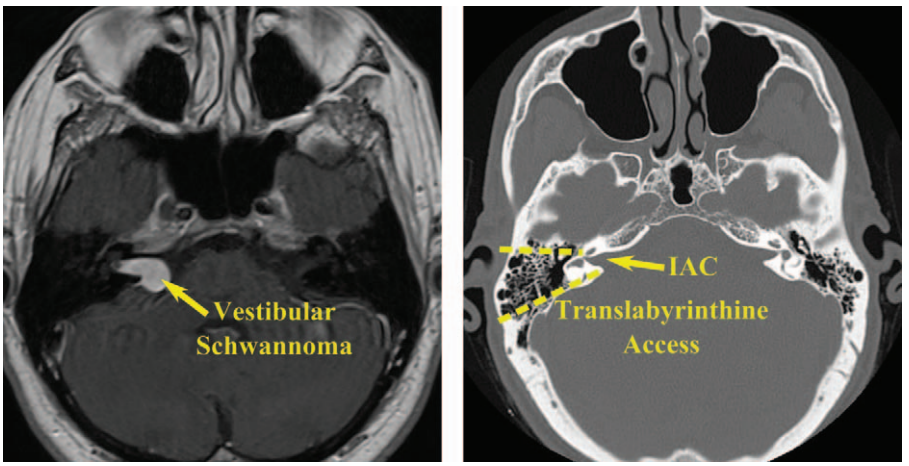

FIG. 1. MRI showing vestibular schwannoma in the internal auditory canal (*left*) and extending into the cerebellopontine angle. Tumors of this size are typically removed using the translabyrinthine surgical approach, which requires extensive bone removal in the mastoid and labyrinth to access the internal auditory canal, as shown in the CT scan on the *right*. Both images are axial views. Note that these two scans are from different patients. CT indicates computed tomography; MRI, magnetic resonance imaging.

finesse for the crucial work of opening the IAC and resecting the tumor.

Central to this robotic approach is the need to precisely identify where the robot is relative to the patient, which can be accomplished using principles of image-guided surgery (IGS). Using IGS techniques, an image space can be registered to its corresponding physical space, thus enabling transformation of relevant anatomy identified in a preoperative image, e.g., computed tomography (CT) scan, to the patient's anatomy intraoperatively. For the proposed application, the anatomy is completely bone encased and does not deform during the intervention relative to the lateral skull. This rigid anatomy enables planning of the approach before surgery using the preoperative CT scan of the patient and transformation of anatomical structures from CT to the patient in the operating room (OR). If a robot is rigidly attached to the skull of the patient, then the anatomical data from the CT can be easily transformed to the robot space.

While still in their infancy, several groups have explored image-guided and robot-assisted surgery for otologic and neurotologic surgery. Federspil et al. (3) used an industrial robot to mill a pocket for a cochlear implantation (CI) bed. Labadie et al. (4–6) developed a method for minimally invasive CI surgery using patient-specific, microstereotactic frames that are manufactured intraoperatively to guide a surgical drill along a path from the lateral skull to the facial recess that avoids vital anatomy and have clinically implemented the system (7). They have also developed image-guided robotic systems for CI surgery (8) and mastoidectomy (9,10). Lim et al. (11) and Xia et al. (12) have also used robots for temporal bone milling. Both of these systems employ a cooperative control approach in which both the surgeon and robot hold the drill and the robot imposes virtual fixtures (i.e., ''no fly zones'') around vital anatomy. Weber et al. (13,14) developed an image-guided robot for drilling a narrow tunnel to the cochlea for minimally invasive CI surgery. Their robot mounts to the surgical table and is registered to the patient using bone-implanted fiducial markers and a highly accurate optical tracking system. Kobler et al. (15,16) have also developed a robot for minimally invasive CI surgery. Their system uses a passive, bone-attached mechanism that can be manually adjusted to align the drill along a specified trajectory.

All of the systems described above use preoperative imaging along with accurate hardware and guidance systems with the goal of improving otologic surgery by taking advantage of the precision of surgical navigation, stereotactic frames, and robotics. Building on much of the work described above, the purpose of the present work is to develop and test a robotic platform for assisting with extensive bone milling during translabyrinthine access to the IAC for VS resection. An overview and intial testing of the first version of this system was previously described by our research group (10). In this article, we provide further testing of the image-guided robotic system on fresh cadaver heads using the full clinical workflow and specifically target deeper drilling volumes through the dense bone of the labyrinth for the translabyrinthine approach to VS. Furthermore, we provide the first report of milling time for the robot-assisted approach, which is one of the motivations for using the technique and was previously not reported.

MATERIALS AND METHODS

Overview of Robotic System and Surgical Workflow

The image-guided robotic system is shown in Fig. 2A. It is a custom-developed four degrees-of-freedom robot that mounts directly to the patient's skull using an intermediate positioning frame (see Fig. 2, B and C). The planning process begins with automatic segmentation of vital anatomy (e.g., facial nerve, chorda tympani) in the preoperative CT scan using previously developed methods (17,18). Using the locations of the vital anatomy as boundaries, the volume of bone to be removed by the robot is manually delineated on the CT scan using custom

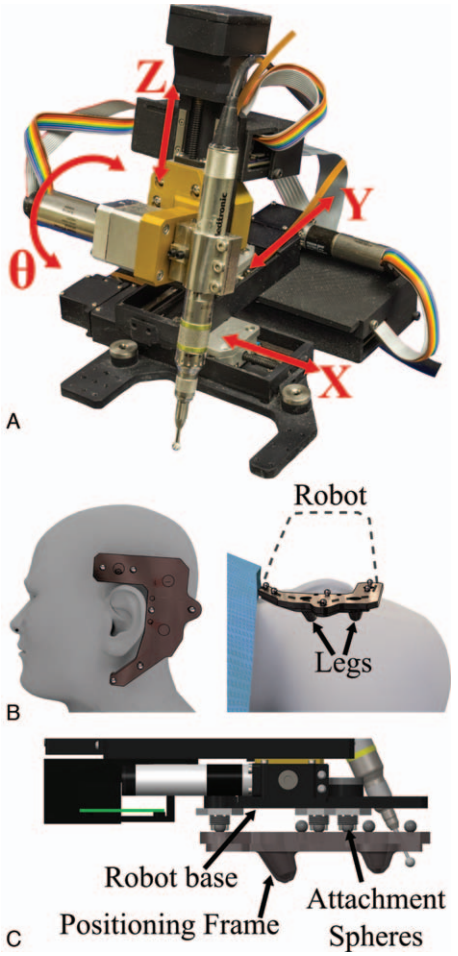

FIG. 2. *A*, Bone-attached robot developed for temporal bone milling. The robot has four degrees-of-freedom (three linear joints: "X", "Y", and "Z" in the figure; and one rotational joint: "θ" in the figure) and guides a surgical drill based on a preoperative plan. *B*, *C*, A positioning frame is used to attach the robot to the patient. The positioning frame is attached to the patient's skull using cranial plating screws and the robot mounts to the top of the frame. The positioning frame contains spheres that serve as both attachment points for the robot as well as fiducial markers for registration. Part (*C*) is a side view of the positioning frame and robot.

software. Automated adjustments are then made to account for the particular cutting burr size. For example, if the burr cannot fit in a particular region of the segmented target volume without touching un-targeted bone, that region is removed from the final target volume. This modified target volume, along with the segmentations of vital anatomy are saved for later use with the intraoperative imaging.

In the OR, after standard incision and lifting of soft tissue off of the skull, the positioning frame (Fig. 2, B and C), is attached rigidly to the patient's skull using three cranial plating screws. The positioning frame serves as the intermediate attachment piece between the patient and the robot. It contains six metal spheres—three spheres onto which the base of the robot mounts and three additional spheres that serve as fiducial markers for registration. The locations of the six spheres relative to the robot is known precisely from a calibration process using a coordinate measurement machine (FARO Technologies, Lake Mary, FL). The attachment of the frame requires three small incisions (10–15 mm in length, one per screw) in areas posterior and superior to the exposed mastoid. After the positioning frame is attached, an intraoperative CT scan is acquired using a portable CT scanner. This scan is registered to the preoperative CT using intensity-based registration (19). The fiducial markers on the positioning frame are then localized in the intraoperative CT (20) and used to register the intraoperative CT to the robot coordinate system via point-based registration (21). The preplanned target volume and anatomy segmentations are then transformed to the robot coordinate system using the registration between pre and intraoperative CTs and the registration between the intraoperative CT and the robot. Next, a milling path that will remove the maximum amount of the desired volume of bone without damaging vital anatomy or removing untargeted bone is planned and a corresponding robot trajectory is generated. The robot is mounted to the positioning frame by locking to three of the metal spheres on the top surface of the frame. The robot then begins milling bone under observation of the surgeon through direct visualization or using a surgical microscope. The surgeon can adjust the speed, pause, or abort the procedure at any time. After the bone milling is complete, the robot is removed and the surgeon completes the surgery.

Experimental Methods and Data Analysis

Experiments were performed on fresh cadaver heads donated to Vanderbilt University Medical Center and the full surgical protocol outlined above was followed. Both the preoperative and intraoperative CT scans were obtained using a portable cone beam CT scanner (xCAT ENT, Xoran Technologies, Ann Arbor, MI). The images have an isotropic resolution of 0.4 mm and a volume of 256 × 256 × 142 mm. The bone volume to be removed by the robot for the translabyrinthine approach was segmented and verified by an experienced attending otologist or neurotologist (see Fig. 3). This volume included the mastoid and much of the labyrinth. The volume varied by specimen and included partial or full removal of all three semicircular canals, as specified by the surgeon to provide access to the IAC for VS removal. The planned volume extended to within approximately 1 to 1.5 mm from the IAC, depending on the specific anatomy of the particular specimen.

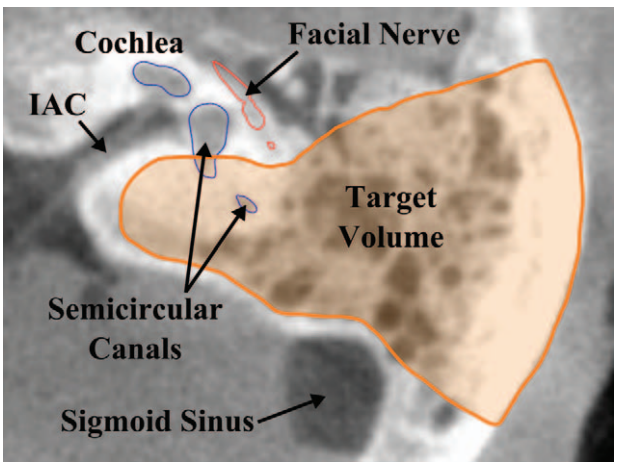

FIG. 3. Axial slice of CT scan showing the segmented middle and inner ear anatomy, including the sigmoid sinus, facial nerve, semicircular canals, cochlea, internal auditory canal (IAC), as well as the target volume of bone to be removed specified by the surgeon.

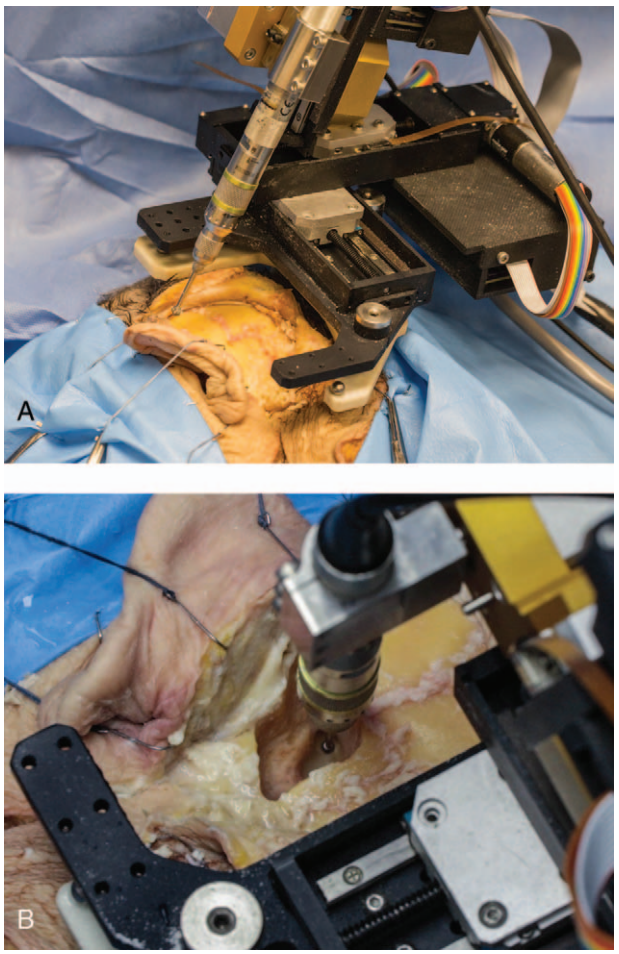

FIG. 4. *A*, Photograph of robot mounted on a cadaver before an experiment and *B*, photograph of drill within mastoid while removing the deeper portion of the volume.

A Midas Rex Legend surgical drill (Medtronic, Minneapolis, MN) and standard fluted spherical cutting burrs were used. A 5 mm burr was used at the start of all experimental trials and further milling was performed with a 3 mm burr in several of the trials. The 3 mm burr was used only in cases in which the smaller diameter enabled removal of substantial additional bone after milling with the 5 mm burr had reached its limit (i.e., the additional access permitted by the size of the 3 mm burr resulted in substantial bone removal deep within the cavity). During the experiment, milling was monitored and irrigation was manually administrated using a suction-irrigation hand piece. Figure 4 shows the robot and positioning frame mounted to a cadaver head before and during an experiment. The milling time was recorded for each experiment. This time value only represents the time spent by the robot milling bone and not the overall procedure time (see discussion below).

A postoperative CT scan was acquired after completion of each experiment to assess the quality of milling. To align the preoperative and postoperative CT scans for verification of the accuracy of the milled cavity, titanium bone screws were inserted into the skull surrounding the surgical area and their locations were determined in both CT scans. These markers were not used for planning but rather served as the ''ground truth'' registration markers for aligning the planned milling with the actual milled volume. Given the location and number of markers, estimates of fiducial localization error (FLE) for the scanner of 0.108 mm root mean square (RMS) (22), and locations of the target points, the registration error between the pre and postoperative scans in the region of the milled volume was estimated to be 0.059 ± 0.004 mm RMS (21). Given this accuracy of the fused images, registering pre to postoperative CT scans is unlikely to contribute any clinically relevant error in assessing the milled cavity.

The volume of bone removed was segmented in the postoperative CT scan and compared with the preoperative plan. The percentage of targeted bone removed was calculated as well as the error between the planned and milled cavity borders. This border error was calculated by creating a mesh of each volume and computing the distance between the surfaces for each point on the planned volume surface. Additionally, the milled cavity was examined under a microscope and the milled volumes and vital anatomy were reviewed in the postoperative CT scan by the surgeon to check for any damage to the vital anatomy.

RESULTS

A total of six trials were performed on five cadaver heads. For one trial, a postoperative CT scan was not acquired due to a malfunction of the CT scanner (the cadaver had to be returned for cremation before the scanner was repaired) so quantitative postoperative measurements are not available for this trial. One additional cadaver head was obtained and scanned; however, the procedure was not performed due to unusual anatomy. More specifically, this specimen's sigmoid sinus was located more anteriorly than normal, which limited the access to the labyrinth through the window between the sigmoid sinus and the facial nerve. In clinical cases, the surgeon would decompress the sigmoid sinus to facilitate access to deeper anatomy; however, we did not

TABLE 1. *Experimental results*

Specimen	Targeted Volume (cm^3)	Percent Removed	RMS Surface Error (mm)[a]	Nerves Preserved	Milling Time
1 (Left)	9.65	97.7%	0.34	Yes	51 min, 11 s
2 (Left)	5.03	95.2%	0.65	Yes	41 min, 56 s
3 (Right)[b]	10.22	-	-	Yes	57 min, 0 s
4 (Left)	5.29	96.7%	0.33	Yes	32 min, 40 s
5 (Left)	9.17	96.0%	0.35	Yes	45 min, 54 s
5 (Right)	11.67	98.0%	0.23	Yes	36 min, 49 s

[a]Root mean square (RMS) error calculated from mean and standard deviation of the absolute value of error along surface of volume.
[b]No postoperative CT scan for this specimen (scanner malfunction; cadaver cremated before scanner was fixed).

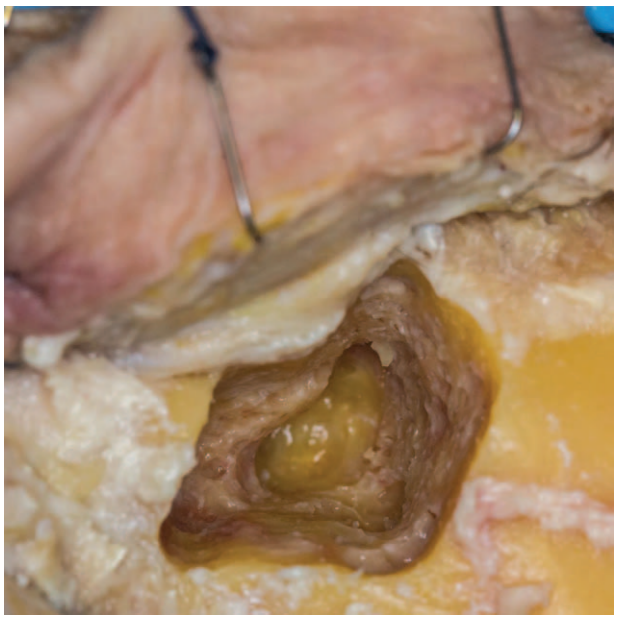

FIG. 5. Photograph of milled cavity for specimen 5 (*left*) after milling was completed.

decompress the blood vessel in this study and thus chose not to perform the milling on this specimen.

Table 1 provides data for each trial, including the targeted volume, percent of bone removed, mean surface error, and milling time. The targeted volume ranged in size from 5.03 to 11.67 cm^3. The milling time ranged from 32.7 to 57.0 minutes. The targeted volume impacts the milling time; however, these values are not directly proportional since the speed at which the robot moves is also affected by the bone density (i.e., the robot is programmed to move faster in more pneumatized areas) and ability to cut with more efficient drill angles. Additionally, iterative refinement of the robot trajectory planning algorithm throughout the study enabled faster bone removal in later trials.

For all experiments, the facial nerve and chorda tympani were preserved. Figure 5 shows a photograph of the milled cavity for Specimen No. 5 (left side). Figure 6 shows slices of the postoperative CT scans for Specimen Nos. 1 and 5 (right side). The outlines on the images indicate the planned milling cavity boundary, which was registered to the postoperative CT scan. Once registered, the two boundaries were compared and the absolute value of the error at each point along the boundary surface was computed.

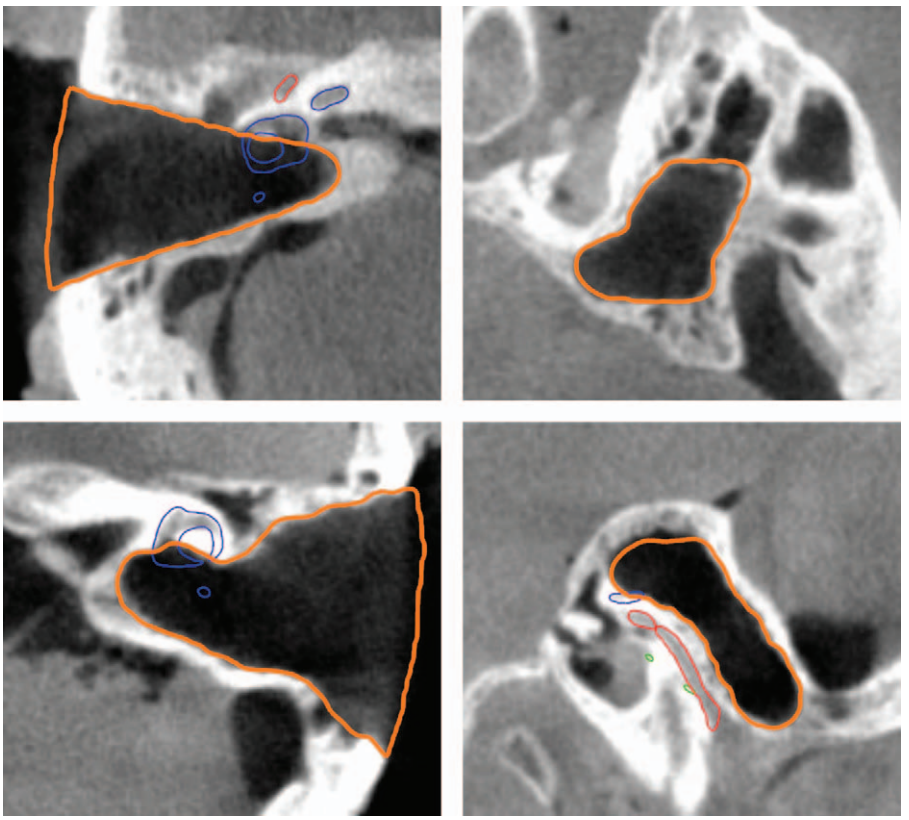

FIG. 6. Slices of postoperative CT scan showing the bone removed by the robot and nearby vital anatomy for Specimen 1 (*top*) and Specimen 5 (*right, bottom*). The *left slices* are axial views and the *right slices* are sagittal views. The specific volume dimensions and planned distances to the nerve were selected on the basis of surgeon preference and could vary based on how large of a mastoidectomy/labyrinthectomy is needed and how close the surgeon wants the robot to approach vital anatomy. CT indicates computed tomography.

TABLE 2. *Proximity of milled cavity to anatomy*

	Closest Distance to Facial Nerve (mm)[a]		Closest Distance to Chorda Tympani (mm)		Closest Distance to External Canal (mm)		Closest Distance to Tegmen (mm)	
Specimen	Planned	Actual	Planned	Actual	Planned	Actual	Planned	Actual
1 (Left)	0.57	0.54	4.35	4.30	2.28	2.03	1.47	0.86
2 (Left)	0.67	0.81	3.32	3.62	1.70	1.75	1.07	1.39
3 (Right)[b]	0.44	-	3.29	-	4.86	-	0.34	-
4 (Left)	0.55	0.51	4.00	3.98	2.13	2.05	0.80	0.72
5 (Left)	0.49	0.48	1.85	1.90	1.99	2.05	0.46	0.52
5 (Right)	1.11	1.34	2.10	2.05	2.05	2.01	0.56	0.54

[a]The closest distance between any point in the planned/milled volume and any point along the surface of the structure.
[b]No postoperative CT scan for this specimen (scanner malfunction; cadaver cremated before scanner was fixed).

Table 2 provides the planned versus actual distances to various key anatomical structures. The distances shown in the table represent the closest distance between any point in the planned/milled volume and any point along the surface of the nerve segmentation. This value was calculated by analyzing the vertices of a three-dimensional mesh of the planned (or removed) volume and the structure. The distances between each vertex of the two meshes were calculated and the minimum value was determined.

DISCUSSION

The results from these experiments indicate that a compact image-guided robot attached rigidly to the skull has the potential to safely perform the bulk portion of bone removal for translabyrinthine access to the IAC for VS removal surgery. The accuracy achieved, in terms of both mean surface error and proximity to vital anatomy, i.e., the difference between planned and actual distance to the facial nerve, is within the required range for this procedure (see Table 2). The exact distance between the milled cavity and various anatomical structures will vary case-by-case according to the required resection volume for access and removal of the tumor. Since the robotic system can use preoperative imaging to know precisely where the vital anatomy is located, the anatomy does not have to be closely approached for identification purposes, potentially enabling larger margins between the removed volume and structures.

The milling times are lower than that typically achieved manually for translabyrinthine access to the IAC in the OR today, even accounting for the additional steps required for the robotic approach. We estimate that the steps in the surgical workflow of the robot-assisted approach that are not part of the convential approach would require an additional 22 to 36 minute depending on the particular patient anatomy. These times are estimated on the basis of our experience in this study as well as experience with a previous clinical study using a bone-attached micro-stereotactic frame for minimally invasive CI that follows many of the same workflow steps (7). However, it is important to note that translation of this approach to clinical use would present additional challenges and, therefore, a fair comparison with current manual bone milling duration in the OR for this procedure is not yet possible. The experiments described in this article were performed in the laboratory by the research group that developed the system so an additional learning curve would be present for new users, which is not accounted for in this data. Also, further bone removal to gain access to the IAC using a smaller diamond burr and surgical pick is required and the time of this component of the surgery, given the access provided by the volume of bone removed by the robot is unknown. Further experimentation, in which the surgeon completes the opening of the IAC, is necessary to evaluate the timing and difficulty of this task. At the least, these preliminary results show that a compact, bone-attached robot can efficiently perform a substantial component of the bone removal.

As described in the Results section, one of the cadaver heads was scanned but the milling was not ultimately performed due to the anterior location of the specimen's sigmoid sinus. It is currently unknown what percentage of the general population (or the subset requiring VS removal surgery) has similar anatomy that restricts the robot from performing the procedure without decompressing the sigmoid sinus. In the future, with a modification of the robot planning protocol, it would be possible to account for these cases. The robot could first mill the volume initially accessible. Then it could be removed, the surgeon could decompress the sigmoid sinus, and then the robot could be reattached and finish the milling.

We encountered several implementation challenges through the course of these experiments and have identified various solutions to improve the ease-of-use of the system moving forward. First, accurate alignment of the positioning frame was difficult in the first few trials because the limited workspace of a compact robot required that it be mounted such that the workspace was approximately centered on the targeted volume of bone to be removed to maximize access. We overcame this challenge by creating a temporary alignment tool that mounts to the frame during the attachment phase and indicates the center of the robot's workspace relative to the frame. Second, segmentation of the target volume of bone to be removed is tedious using the current approach because the surgeon must manually outline the bone in two-dimensional slices of the CT scan. This process is

both time consuming and geometrically disorienting because the surgeon must make mental estimates of how close a two-dimensional segmented slice is to a more superior and/or inferior slice. To make this component of the work flow simpler and more efficient, we are working on automated processes (23) in which a resection volume for robotic translabyrinthine IAC access is computed and used as a starting point for the surgeon who could then manually adjust where necessary. Additionally, our research group's recent work related to computing statistically-driven safety margins around vital anatomy for robotic surgery (22,24) will be integrated into the segmentation process.

Other planned system improvements include: a better surgeon interface and real-time views of the drill tip location in the preoperative CT; redundant safety features such as facial nerve monitoring integrated with the robot; potential verification of the drill tip position based on other sensory information (e.g., force sensing and use of force–density relationship to confirm correct drill location similar to (25)); and optimized selection of burr size to mill as much of the cavity as possible while minimizing the number of burr changes.

CONCLUSION

In this article, we have demonstrated initial feasibility of robot-assisted translabyrinthine access to the IAC for VS removal in fresh human cadavers. The initial results are encouraging; however, we recognize that significant work remains before this technique is clinically viable, including the incorporation of additional safety features to ensure preservation of vital anatomy and improved surgeon interaction with the system. Additionally, the clinical benefits of the robotic approach, in terms of patient outcomes and operating costs over the standard-of-care is currently unknown and must be further evaluated.

Acknowledgments: The authors would also like to thank Dr. Jack Noble for use of his segmentation software and Dr. Louis Kratchman for assistance with making Figure 2.

REFERENCES

1. Carlson ML, Link MJ, Wanna GB, Driscoll CL. Management of sporadic vestibular schwannoma. *Otolaryngol Clin North Am* 2015;48:407–22.
2. Brackmann D, Shelton C, Arriaga MA. *Otologic Surgery*, 3rd ed. Philadelphia: Elsevier Health Sciences; 2010.
3. Federspil PA, Geisthoff UW, Henrich D, Plinkert PK. Development of the first force-controlled robot for otoneurosurgery. *The Laryngoscope* 2003;113:465–71.
4. Labadie RF, Mitchell J, Balachandran R, Fitzpatrick JM. Customized, rapid-production microstereotactic table for surgical targeting: description of concept and in vitro validation. *Int J Comput Assist Radiol Surg* 2009;4:273–80.
5. Labadie RF, Balachandran R, Mitchell J, et al. Clinical validation study of percutaneous cochlear access using patient customized micro-stereotactic frames. *Otol Neurotol* 2010;31:94.
6. Balachandran R, Mitchell JE, Blachon G, et al. Percutaneous cochlear implant drilling via customized frames: an in vitro study. *Otolaryngol Head Neck Surg* 2010;142:421–6.
7. Labadie RF, Balachandran R, Noble JH, et al. Minimally invasive image-guided cochlear implantation surgery: First report of clinical implementation. *The Laryngoscope* 2014;124:1915–22.
8. Kratchman LB, Blachon GS, Withrow TJ, Balachandran R, Labadie RF, Webster RJ. Design of a bone-attached parallel robot for percutaneous cochlear implantation. *IEEE Trans Biomed Eng* 2011;58:2904–10.
9. Danilchenko A, Balachandran R, Toennies JL, et al. Robotic mastoidectomy. *Otol Neurotol* 2011;32:11.
10. Dillon NP, Balachandran R, Fitzpatrick JM, et al. A compact, bone-attached robot for mastoidectomy. *J Med Dev* 2015;9: 031003.
11. Lim H, Han JM, Hong J, et al. Image-guided robotic mastoidectomy using human-robot collaboration control. In: 2011 IEEE International Conference on Mechatronics and Automation 2011 Aug 7; 2011. (pp. 549–554). IEEE.
12. Xia T, Baird C, Jallo G, et al. An integrated system for planning, navigation and robotic assistance for skull base surgery. *Int J Med Robotics Comp Assist Surg* 2008;4:321–30.
13. Bell B, Stieger C, Gerber N, et al. A self-developed and constructed robot for minimally invasive cochlear implantation. *Acta Otolaryngol* 2012;132:355–60.
14. Bell B, Gerber N, Williamson T, et al. In vitro accuracy evaluation of image-guided robot system for direct cochlear access. *Otol Neurotol* 2013;34:1284–90.
15. Kobler JP, Kotlarski J, Öltjen J, Baron S, Ortmaier T. Design and analysis of a head-mounted parallel kinematic device for skull surgery. *Int J Comp Assist Radiol Surg* 2012;7: 137–49.
16. Kobler JP, Nuelle K, Lexow GJ, et al. Configuration optimization and experimental accuracy evaluation of a bone-attached, parallel robot for skull surgery. *Int J Comput Assist Radiol Surg* 2016;11:421–36.
17. Noble JH, Warren FM, Labadie RF, Dawant BM. Automatic segmentation of the facial nerve and chorda tympani in CT images using spatially dependent feature values. *Med Phys* 2008;35: 5375–84.
18. Noble JH, Dawant BM, Warren FM, Labadie RF. Automatic identification and 3-D rendering of temporal bone anatomy. *Otol Neurotol* 2009;30:436.
19. Maes F, Collignon A, Vandermeulen D, Marchal G, Suetens P. *IEEE Trans Med Imaging* 1997;16:187–98.
20. Wang MY, Maurer CR, Fitzpatrick JM, Maciunas RJ. An automatic technique for finding and localizing externally attached markers in CT and MR volume images of the head. *IEEE Trans Biomed Eng* 1996;43:627–37.
21. Fitzpatrick JM, Sonka M. *Handbook of Medical Imaging, Volume 2. Medical Image Processing and Analysis*. Bellingham: SPIE Press; 2000.
22. Dillon NP, Siebold MA, Mitchell JE, et al. Increasing safety of a robotic system for inner ear surgery using probabilistic error modeling near vital anatomy. *SPIE Medical Imaging 2016 (97861G-97861G)*. International Society for Optics and Photonics; 2016.
23. McBrayer KL, Wanna GB, Dawant BM, Balachandran R, Labadie RF, Noble JH. Resection planning for robotic acoustic neuroma surgery. *SPIE Medical Imaging 2016 Mar 18 (978608-978608)*. International Society for Optics and Photonics; 2016.
24. Siebold MA, Dillon NP, Webster RJ, Fitzpatrick JM. Incorporating target registration error into robotic bone milling.*SPIE Medical Imaging 2015 Mar 18 (94150R-94150R)*. International Society for Optics and Photonics; 2015.
25. Williamson TM, Bell BJ, Gerber N, et al. Estimation of tool pose based on force–density correlation during Robotic drilling. *IEEE Trans Biomed Eng* 2013;60:969–76.